SVU-International Journal of Engineering Sciences and Applications (2023) 4(2): 243-259
Print ISSN 2785-9967| Online ISSN 2735-4571
DOI 10.21608/svusrc.2023.213317.1127

# Influence Parameters on the Essential Work of Fracture of 5754-H111 Aluminum Alloy Plate: Comparative Study

**Al-Shimaa H. Kamal[1], Nouby M. Ghazaly[1], Mohammed Y. Abdellah[1,2,□], Abo-El Hagag A. Seleem[3] and G. T. Abdel-Jaber [1, 4]**

**Abstract:** Aluminum alloy 5754 is a medium strength alloy with excellent corrosion resistance especially to seawater and industrially polluted atmospheres. Aluminum alloy 5754-H111 shows good cold formability, high fatigue strength and fair machinability. The present work aims to develop the test specimen to obtain the Essential Work of Fracture EWF which based on the Ligament yielding observed to occur at the peak of the load-displacement curve. It Follow this, necking and tearing occur in the softening region. The plastic zone, however, expands as a result of the non-essential work of fracture being dissipated in the tearing process after yielding. For studding the effect of stress raiser on Essential Work of Fracture three procedure applied, First at high test speed second with holes third at pre-stress .This work contributes to the overall goal to model fracture behavior and crack propagation .Investigation the adhesion properties by static tests concerned with stress lines concentrations on different material volume have been achieve in the obtained results .The EWF method achieved 273 KJ/m² for 5 mm thickness and 63 KJ/m² for 1.8 mm thickness these values. The strain rate test achieved high value of EWF is measurement as 330 kJ/m²for 5mm and 28 kJ/m²for1.8 mm. By applying holes near the crack, the toughness increased which has been presented at the high value of EWF measurement compared without holes that the 5 mm specimen's thickness achieves 380 KJ/m² and for 1.8 mm thickness 110 KJ/m². On pre-stress 20% the EWF measured 250 kJ/m²for 5mm and 20 kJ/m²for1.8 mm and continues for pre-stress 30% EWF measured 230 kJ/m²for 5mm and 15 kJ/m²for1.8 mm. Also pre-stress 40%The EWF measured 210kJ/m²for 5mm and 10 kJ/m²for1.8 mm. For pre-stress 50% the EWF achieve lowest value measured as 190 kJ/m²for 5mm. The reduction of prestress values related to the broken average of atomic bonds due to increase the pre- load applied on the specimens.

**Keywords:** Aluminum alloy, Stress raiser, EWF, fracture toughness.

## 1 Introduction

***Nomenclature***

| | |
|---|---|
| $\beta$ | Plasticity shape factor |
| $\beta_p$ | Geometric shape factors related to the plastic zone during tearing after necking |
| $\beta_y$ | Geometric shape factors related to the plastic zone during ligament yielding |
| $\beta_{wp}$ | Plasticity shape factor |
| $K$ | stress concentration factor for static load |
| $L$ | Ligament length |
| $L_\circ$ | the initial gauge length |
| $L(t)$ | the length of the specimen at time t |
| $\sigma$ | the average stress |
| $t$ | Thickness of the specimen |
| $v$(t) | is the cross-head speed |
| w | Sample width |
| $W_f$: | Total strain energy attributed to fracture |
| $we$ | Essential work of fracture in the elastic zone |
| $W_p$ | Work of the tearing and necking |
| $wp$ | Non-essential work of the fracture |
| $W_{pp}$ | Relative plastic energy in tearing and necking |
| $W_y$ | Elastic energy of the elastic and yielding ligament length |
| $wy$ | Essential work of fracture in the elastic zone |
| $W_{py}$ | Relative energy in plastic and yielding of ligament length |

Al-Mg aluminum alloys, denoted by the 5xxx series, have a relatively low strength but a very good formability. Only work hardening can make this family of alloys stronger[1]. The solid-solution strengthening that magnesium provides gives these alloys their strength. Zirconium, manganese, and other alloying elements are

Received: 25 May 2023/ Accepted: 10 June 2023
□Mohammed Y. Abdellah, mohammed_abdalla@eng.suv.edu.sa
1.Mechanical Engineering Department, Faculty of Engineering, South Valley University, Qena, 83523, Egypt
2. Mechanical Engineering Department, College of Engineering and Islamic Architecture, Umm Al-Qura University Makkah, KSA
3. Sun Miser Petroleum Company, Egypt.
4. New Assiut university of Technology (NATU), Assiut, Egypt

added to manage the grain and subgrain structures, which also aid in strengthening [2]. According to Broberg [3-5] the non-elastic zone at the crack tip can be separated into two regions: an outside region where plastic deformation accommodates the significant strains from the end region, and a fracture process end region. When plastic deformation occurs in ductile material, it occurs mostly in the outer region, which is larger than the end region. The terminal region of thin sheets made of ductile material can be recognized by necking. The job completed in the final area can be viewed as autonomous and is therefore referred to as vital work. Plane stress is a reasonable assumption for thin sheets, however in this situation; the necking area depends on the sheet thickness. Therefore, because it depends on the thickness of the sheet, the essential work is not a true material constant. The geometry of the test condition affects the plastic deformation in the outer region. Consequently, the related plastic work is not a constant of the material. The assumption of a crack and the relationships among the length of the crack, the material's natural resistance to crack propagation and the stress at which the crack propagates rapidly to cause structural failure are made. Abdellah et al[6] applied a two fracture method, essential work of fracture method and compact tension test, using a two different thickness to investigate the surface energy JIC and the essential work of fracture for 5754-H111 aluminum alloy . He also created a straightforward finite element numerical model using the essential work of fracture (EWF) to forecast the parameters of EWF .Although the sample was measured in millimetres, the findings of the experiment and the suggested model were in good agreement.[7]. According to Betegon et al[8] investigation on the mechanical damage of the 5754-H111 aluminum alloy, microcavities or microvoids are mostly responsible for damage and fracture. Using three distinct setups for quasi-statics, medium, and high strain rates, Ezio Cadoni et al[9] examined the impact of strain rate on the mechanical characteristics in tension of a commercial aluminum alloy AA7081The results demonstrate a strain rate sensitivity of the uniform and fracture strain as well as a moderate decrease in cross-sectional area at fracture with increasing the strain rate. The stress increases at strain rates between $10^{-3}$ and$10^{3}$ $s^{-1}$. These experimental findings have led to the determination of the Johnson-Cook constitutive low's necessary parameters.

A simplified plane-symmetrical two-dimensional finite element model for a SHPB with a plate specimen constructed of an elastic material is initially established in Samsul Rizal et al[10] .'s work. the impact test involves the use of a strain gauge put on the specimens to monitor strain. The numerically predicted and experimentally measured load and a sample strain can then be compared. This study also covers the benefits and drawbacks of the experimental technique while also describing the equipment and instrumentation. For evaluation of the fracture mechanism and the effects of strain rates on the materials, a fracture graph is acquired using a scanning electron microscope on the center of the specimens

.In the strain rate range of 0.001 $s^{-1}$ to 850$s^{-1}$, Singh et al[11, 12]investigated the dynamic compressive and tensile behaviour of the aluminium alloy AA6063–T6. Tanimura et al[13]used a sensing block type high speed material testing system to investigate the dynamic behavior of several types of aluminum alloys. Oosterkamp et al[14]examined the strain rate sensitivity of two commercial aluminum alloys, AA6082 and AA7108, in peak temper T6 and overaged T79 incompression and in a wide range of strain rates, from 0.1 to 3000 s1, at room temperature and high temperature (around 500 C). They found a tendency of negative strain rate sensitivity for strain rates greater than 2000 s1, which was caused by the localization of strain on. Extruded aluminum alloys AA6060, AA6082, AA7003 and AA7108 in T6 temper were studied in an experimental campaign by Chen et al[15] for a wide range of strain rates. Using a Split Hopkinson Tension Bar device, tensile tests at high rates of strain were conducted. They emphasized that the AA6060-T6 and AA6082-T6 showed only marginal sensitivity to the strain rate, and as a result, these alloys may be accurately characterized as rate-insensitive. A substantial sensitivity to strain rate was discovered for the alloys AA7003-T6 and AA7108-T6, which was then taken into account in simulations. Fatigue and fracture are fundamentally two different things. Considering that stress raisers are where fatigue failures almost always start, reducing stress concentration is crucial. Therefore, a comprehensive understanding of stress concentration aids designers in identifying stress raisers and taking the appropriate action to reduce stress concentration[16] The issue of stress concentration is one that designers shouldn't ignore. Practically speaking, the high stress concentration at a hole's edge is very significant. When a ship's hull is bent, the decks experience tension or compression, and the holes experience a significant amount of stress. The metal may eventually become fatigued at the overstressed region and develop fatigue cracks that lead to fracture under the cycles of stress created by waves. In plates with holes, brackets, grooves, and slits, the stress concentration is crucial [17] . Bracket is a crucial component, causes

significant cycle fatigue and reduces the lifespan of the bracket. A factor known as the stress concentration factor is used to quantify stress concentration. The ratio of the highest stress to the nominal stress is known as the stress concentration factor. The simple stress distribution no longer applies once a machine component alters the geometry of its cross-section, and a different stress exists in the area around the discontinuity. Stress concentration refers to this irregularity in the stress distribution brought on by sudden changes in its shape. In the presence of fillets, notches, surface roughness, keyways, holes, etc., it happens for all types of stresses[18] The main challenge to stopping crack propagation is lowering the stress concentration factor near the crack tip. The crack tip stop hole is used to reduce the fracture tip's stress singularity and extend the structure's fatigue life. According to Song et al [19] longer fatigue lifetimes were obtained by drilling a hole at the crack tip with larger stop hole sizes. In order to better understand the impact of hole diameter and cold expansion on the improvement of fatigue life, Ghfiri et al[20]investigated certain pre-cracked specimens under fatigue loading. The impact of the stress raiser in the aluminum plate on the finite element was researched by Abdullah et al[21] . To gauge and simulate the vibration response of aluminum cantilever plates with and without holes, modeling FEM was created. The tensile test characteristics of standard aluminum specimens are used to run the finite element model. The results demonstrate the natural frequencies and damping ratios for the notch and unnotch aluminum plate shape modes at three different scales. It was found that the value of the damping ratio increased with hole diameter. A reliable form mode prediction is provided by finite element modeling.

Notably, the positions of the holes in relation to the crack were thoughtfully planned with various distance factors to enable quantitative measurement. In the impact experiment, the Split-Hopkinson pressure bar (SHPB) and crack propagation gauges (CPGs) were used, and data on the crack fracture phenomenon and propagation velocity were gathered. A numerical model was constructed utilizing appropriate damage criteria and AUTODYN software[22-26] in order to explore the mechanism of the holes' impact on crack propagation. Fei Wang et al [27] study the effect of the holes on dynamic crack propagation was investigated using a experimental–numerical method. SHPB experiments were conducted with a crack propagation gauge test system, and the finite difference code AUTODYN was applied in determining the mechanism of the holes' effect. Both experimental and numerical results demonstrate that the holes have a suppressing action on the moving crack; as the two-hole spacing decreases, the suppressing action intensifies.

Also Abi-Akl and Mohr [28] examined the impact of pre-stress on the plasticity and fracture of AA6451-T4 aluminum sheets. Selected specimens were pre-stretched 2.0% and 5.0% before all specimens underwent artificial ageing at 180 °C for 20 minutes as part of a number of material tests. The results of uniaxial tension testing in the direction of rolling revealed the same patterns as those noted by Furu et al[29] Specifically, a higher level of pre-stretching results in higher yield strength for alloys in the underaged temper. The highest pre-stretching level showed less work-hardening, and the final tensile stress was attained at a lower plastic strain. The failure strain measured on the surface in several notch tension tests was lower for the highest level of pre-stretching, according to the strain fields determined by digital image correlation analysis.

By using models based on nanostructures and tests, Henrik Granum et al[30] investigate the impact of pre-stretching on the mechanical behavior of three 6xxx series aluminum alloys. With no discernible loss in yield stress, work-hardening, or ultimate tensile stress, the uniaxial tension tests reveal that the alloys pre-stretched 4.0% demonstrate much greater ductility than the alloys pre-stretched 0.5%. The enhanced ductility is also demonstrated in the RHS profile crushing tests, where the alloys with pre-stretching of 4.0% show fewer cracks than those with pre-stretching of 0.5% at equivalent energy absorption. The limiting factors in energy absorption difficulties, pre-stretching is an effective solution, as evidenced by the specific mean force in the crushing tests being less than 5% lower for the alloys that were pre-stretched 4.0%. According to the microstructure evolution predicted by NaMo, the increased contribution from dislocations in the 4.0% pre-stretched alloys, compared to the 0.5% pre-stretched alloys, more than makes up for the decreased contribution from precipitates to the yield stress. The alloy's capacity to work-harden is marginally hampered by the dislocations produced during pre-stretching. The 4.0% pre-stretched alloys appear to be overaged based on the increased precipitation kinetics seen for higher pre-stretching levels, which is compatible with the observed increase in ductility. According to Al-Rubaie et al.[31] discuss pre-straining deformations of 1-7% result in sliding grains and persistent slip bands (PSBs), which reduce the fatigue life of a 7050-T7451 aluminum alloy plate. The reduction in fatigue life grew as the pre-straining level. A few reports have suggested that pre-deformation or pre-straining is detrimental to the

fatigue performance and fatigue life of metallic materials. Brancoa et al.[32] reported that the heterogeneous distribution of dislocations, such as dislocation stacking at slip bands and at grain boundaries, due to the pre-tensile deformation of the 7050-T6 aluminum alloy accelerating the damage accumulation at the grain boundaries, and reduced its fatigue life after pre-tensile deformations of <8.According to Froustey et al.[33] a rise in pre-tensile deformation considerably reduced the 2017A-T3 aluminum alloy's residual fatigue life. Y. Abdullah[34] presents the damage criteria for the same alloy 7075 T6 using an explicit dynamic finite element model using static tensile damage, where the S-N CURVE AND surface damage under fatigue are well-represented. .According to White et al.[35] a 1% pre-tensile deformation reduced the fatigue life of a friction-stir-welded joint made of the AA7050 alloy. As the pre-tensile deformation increased from 5% to 12%, Chiou et al[36] discovered that the cyclic softening effect during the fatigue loading process of SUS 430 stainless steel increased along with the increase in the pre-tensile deformation, significantly shortening its fatigue life under symmetric tension and compression fatigue loads. Pre-straining has a detrimental effect on the fatigue life of CP800 steel, according to Sun[37].

Aluminum alloy 5754-H111 alloy has been usually studded by the researchers as water sea corrosion resistance. The investigation of this study is discussed of fracture behavior and crack propagation of Aluminum alloy 5754-H111 test specimen under ductile damage using linear elastic fracture mechanics to obtain, First the fracture toughness presented in Essential Work of Fracture [EWF], Second discuss the effect of stress raiser which created by cortical defects, changing in stiffness or cracks by comparative studies with high test speed second with holes third at pre-stress. This comparative present the higher level of stress focused on ligament length, Third look into the failure modes and fracture topography in ductile damage

## 2 Martial

Egypt Alum.Co. Provided us commercial aluminum 5754-H111 alloy specimens. These elements are what make up the A5754-T alloy's chemical makeup, as seen in table 1.

Table 1 chemical composition of Aluminum alloy[38]

| Zn | Cu | Mn | Si | Fe | Mg | Cr | Ti | Al |
|---|---|---|---|---|---|---|---|---|
| 0.2 | 0.1 | 0.5 | 0.4 | 0.4 | 2.6-3.6 | 0.3 | 0.15 | Bal. |

The aluminum alloy 5754 is highly influenced by these chemicals, which contribute to its exceptional corrosion resistance, especially in the presence of seawater and industrially polluted atmospheres. It is an alloy with middling strength. The alloy has undergone shaping-induced work hardening, as indicated by the symbol H111. Aluminum alloy 5754-H111 exhibits high fatigue strength, acceptable machinability, and good cold formability. The 5xxx series of alloys with increased strengths includes this one. Because of this, 5754-H111 is a good choice for applications including flooring, shipbuilding, and buildings that employ chemicals or nuclear power. It is frequently used in the interior body panels and structural components of automobiles[39]. By using the ASTM E399-81 standard tension test as indicated[40]. The material qualities described by these data are listed in Table 2..

Table 2. Mechanical properties of Al 5754-H111 alloy.

| Yield strength (MPa) | Ultimate tensile strength (MPa) | Young's modulus (GPa) | % elongation |
|---|---|---|---|
| 153.9 | 265 | 68 | 1.2 |

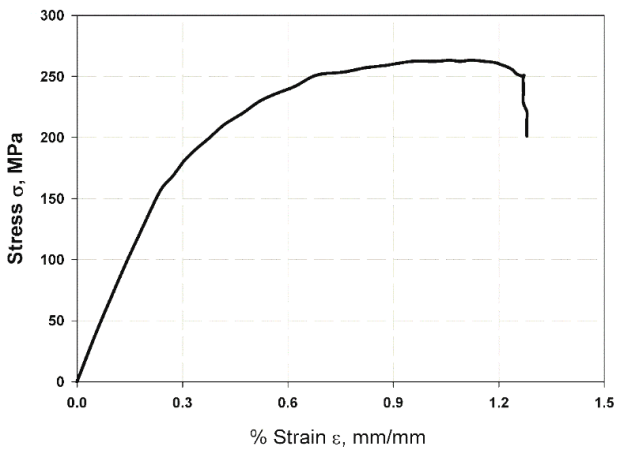


**Fig.1 stress and strain relation for Aluminium alloy**

### 3. Analytical method for essential work of fracture

In recent years, the essential work of fracture (EWF) method has been used more frequently to assess the fracture toughness of thin material films [41]. According to the EWF method, there are two components to the total energy (wf) required to fracture a notched specimen: the essential work (we), which is used to create new surfaces in the so-called fracture process zone, and the non-essential work (Wp), which is used to plastically deform the area surrounding the process zone. In light of this, [7] it is possible to define the specific work, wf, as the union of the two terms below.

$$W_f = \int_0^{\delta} W_p \, d\,\delta \quad (1)$$

$$W_f = W_e + W_p \quad (2)$$

$$W_f = W_e + \beta W_p \quad (3)$$

Fig. 1 depicts the EWF technique used to crack the surface of typical DENT specimens. When the two plastic zones formed on the crack sites are in contact with one another, Ligament L totally yields to the maximum force supplied to the specimen[42]. When the ligament entirely breaks due to ductile cracks, the load versus displacement curve is shown as shown in Fig. 2[41].

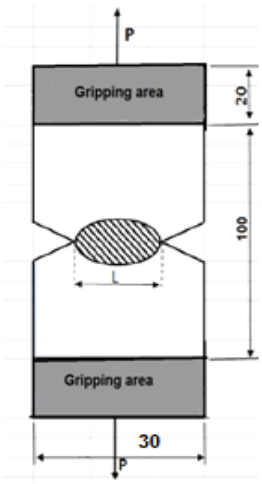


**Fig. 2 Double-edge notched specimen with a plastic zone [[43, 44]].**

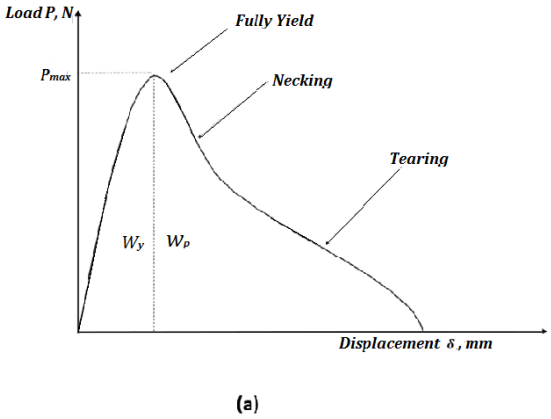


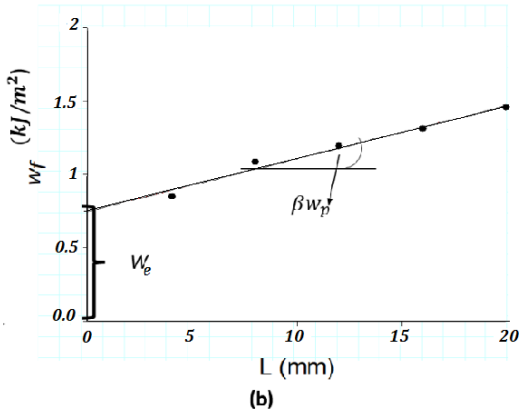


**Fig.3. EWF data (a) load–displacement curve and (b) EWF fitting [44].**

$w_e$ Represents the surface release work in the crack process zone, wp stands for the plastic deformation zone behind the fracture process zone, and we stands for the crack tip instability. Additionally, the failure displacement is. The surface release work we, for a given specimen thickness, relies on ligament length L, which is noteworthy. "Plastic work" is defined as volume energy proportionate to volume ($L^2t$) (wp). The equation for energy is obtained by dividing Eq. (2) by the ligament area Lt:

$$w_f = \frac{W_f}{Lt} = w_e + \beta\, w_p L \quad (4)$$

Considerations include the fracture's unique non-essential work, the plastic deformation shape factor, and the plastic work per unit volume of the plastic deformation zone in front of the crack tip. The development of the crack surface also depends on the surface release energy. The link between wf and ligament length L is shown by equation (3). The range of ligament lengths required for effective EWF testing to

begin the crack surface developing depends on the plastic work per unit volume of the plastic deformation zone in front of the fracture tip. Equation (3) presents a linear regression that links wf to ligament length L. The "thumb rule" of Cotterell and Reddel[45]

$$l_{min} = (3-5)t < l < l_{max} = \frac{W}{3} \quad (5)$$

We are the positive intercept at L = 0 for the specific EWF. By fitting the data linearly with the fracture wp auxiliary work, the slope of the regression line may be computed (see Fig. 2b). After a force is applied and the ligament fully yields, Eq. (2) for a DENT specimen can be rewritten as follows:

$$W_f = W_y + W_{pp} \quad (6)$$

The mechanical energy in the elastic zone and the plastic energy utilized for necking and subsequent tearing, respectively, are denoted by Wy and Wpp, as shown in Fig. 2 a. Using Eq. (4), the plastic zone of EWF Wpp connected to tearing before necking forward of the crack tip and the elastic zone of EWF Wey associated with crack initiation can be divided into two zones, as illustrated below:

$$W_e = W_{ey} + W_{epp} \quad (7)$$

Following are the divisions of the slope:

$$\beta W_p = \beta y\, w_{py} + \beta p\, w_{pp} \quad (8)$$

Where, respectively $\beta y$ and $\beta p$ are geometric slope parameters associated with plastic zone during ligament yielding and tearing after necking

## 4. Stress Raiser procedures

### 4.1. Strain Rate

A material's change in strain with respect to time is known as the strain rate. The strain rate can be stated as a single number when a straight tensile test specimen is loaded.

$$\dot{\epsilon}(t) = \frac{d\epsilon}{dt} = \frac{d}{dt}\left(\frac{L(t)-L_0}{L_0}\right) = \frac{v(t)}{L_0} \quad (9)$$

Where $v(t)$ is the cross-head speed, $L_0$ the initial gauge length and $L(t)$ the length of the specimen at time t.

The strain rate for notched specimens varies according to the location inside the specimen. It is practical to define the displacement rate of the test machine's cross-head when classifying test speeds. Calculating the strain rate by multiplying the cross-head speed by the measurement length is possible, but the result may be deceptive. The material experiences different, significantly higher strain rates in the vicinity of the notch and at the crack's tip than would be detected by a typical extensometer. Noda, et al[46] address the strain rate concentration for DENT specimens at the root of the notch.

### 4.2. Hole

The issue of stress concentration is one that designers shouldn't ignore. The relationship between the maximum stress that occurs and the average effort that should occur is defined as the stress concentration factor. This relationship is determined by experimental or analytical methods and is presented in graphical form for ease of understanding. The stress concentrators are geometrical irregularities. It is notable that the high stress concentration found at the edge of a hole causes an increase in the average effort that should be present in regions near these discontinuities. Notably, the large stress concentration at the hole's edge has significant practical implications. When a ship's hull is bent, the decks experience tension or compression, and the holes experience a significant amount of stress.

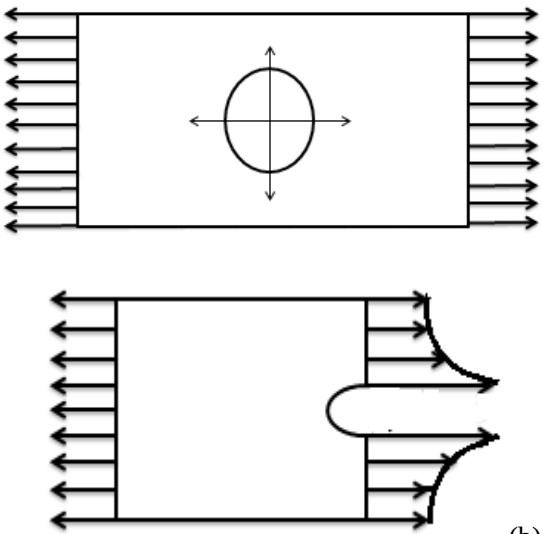


**Fig 4 . Stress distribution for a plate subjected to tensile load (a)Away from the hole; (b) in the section of central hole[47]**

In our study the selection of hole dimension present in fig [4]. Predicting the flow stress the maximum stress concentration has been found at the crack tip and the edge of hole so the total stress concentration at the crack tip will be reduce due to the effect of hole .This reduction will vary according to ligament length.

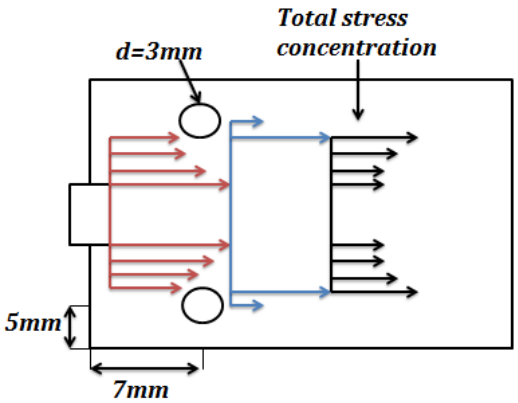


**Fig 5. Hole made and stress concentration**

#### *4.2.1 Stress concentration factors*

The relationship between the actual maximum real stress in the discontinuity and the average stress, which is calculated using the equation 10, is the stress concentration factor for static load[19]

$$K = \frac{Actual\ maximum\ stress}{Avarage\ stress} \qquad (10)$$

The fundamental equations can be used to calculate the average stress, which is specified in terms of the kind of load being applied to the element. Equation 11 is used to compute this value in the event of an axial load that causes tension or compression.

$$\sigma = \frac{Axial\ Force}{Cross\ section\ area} \qquad (11)$$

The type of discontinuity, the geometry of the discontinuity, and the type of load are the stress concentration factors.

### 4.3. Pre-stress

By reducing the cohesive energy between the nucleation of precipitates, the use of pre-stressing is harmful to the fatigue performance and fatigue life of metallic materials. The major phases in the procedure were estimating the 265 Mpa ultimate tensile strength from uniaxial tensile tests with various amounts of pre-stretching (20%, 30%, 40%, and 50%) were utilized to study the impact of pre-stretching on mechanical behavior.

## 5. Experimental Setup

A universal testing apparatus (type WDW-100) with a 20 kN maximum capacity was used for the test at transverse speed of 2 mm/min, which was carried out at room temperature. The DENT specimens stood out when milled because their symmetry prevented specimen buckling during loading. The buckling effect drastically reduces the load, which changes how the load displacement curve behaves[48-51]. The load was applied on both sides of the specimen to complement failure, and the load and displacement were recorded. The test as depicted in Fig. 1 was performed in accordance with[52] and five specimens were used to measure the EWF values for both thickness[50] and the number of specimens for each ligament was three. The various ligament lengths of 4, 6, 10, 12, and 14 mm with a 30 mm width. The specimen was cut with a CNC milling machine. The cracks were cut with a sharp blade of 1 mm thickness according to[50].

## 6. Results and discussion.

### 6.1 Essential work of fracture

The force-displacement curves for 5 mm and 1.8 mm aluminum DENT specimens measured using EWF at room temperature are shown in Figs. 6 a and b. The curves increase linearly up to a certain point, at which time an oscillation that denotes the flow range occurs, and they then continue to increase until they reach their peak value (full flow). Following that, eventual failure and ductile cracking take place. Similar geometries can be seen in the load displacement curves as a function of ligament length. The area under the force-displacement curve is a measure of the total energy Wf held within the cracked specimen. Equation (1) is used to determine this area's size. Because there is more material to be deformed, as the ligature length rises (middle part), the internal work also increases. As the material's resistance rises, the crack then spreads throughout it (the length of the fracture zone grows as the ligature length grows).A shorter ligament results in a longer fracture starting length a0. Plotting the area under the linear intercept of the force displacement curve provided the elastic work of fracture, or wy. After that, the area of the ligament section (Lt) was divided by the total work Wf under the curve, resulting in a polarised relationship between the total work Wf and each ligament as shown in Fig. 7. Figures 7a and b, for DENT with 5 mm and 1.8 mm thickness, respectively, illustrate the linear regression of the overall work performed per ligament area. It was discovered that the (we) intersection point between the extension of the linear regression data and the y axis was separated, and that it was 273 kJ/m2 for a 5 mm thick plate and 63 kJ/m2 for a 1.8 mm thick plate, respectively. This was proof that the thickness is a crucial factor in determining how sensitively a fracture will occur. The greater value is a result of MgO production during fracture propagation, which is brought on by oxygen entering the crack. For 5 mm thick plates, the MgO particles were dispersed over the crack surfaces [53]. These solid tiny particles bridge the fissure surfaces, slowing the propagation or progress of the breach. Due to the narrow crack surface having little to no bridging by the crack, the fracture toughness at the thin thickness was relatively low at 63 kJ/m2.Additionally, the Si would fracture, adding to the fracture[54]. This is due to the fracture

toughness' thickness sensitivity; even at thin thicknesses, there was more localized stress. Net tension was the mode of failure for all specimens, measuring 5 mm and 1.8 mm, respectively, as illustrated in Fig. 18(a),(b).

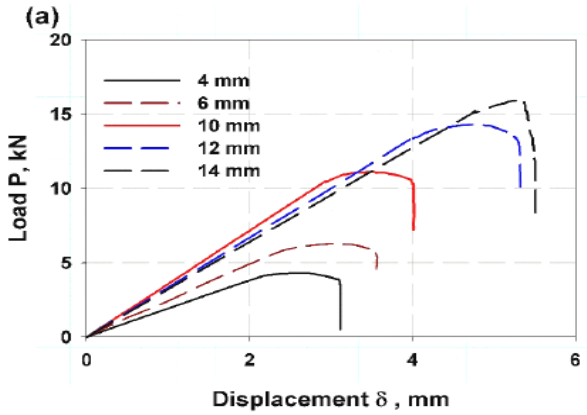


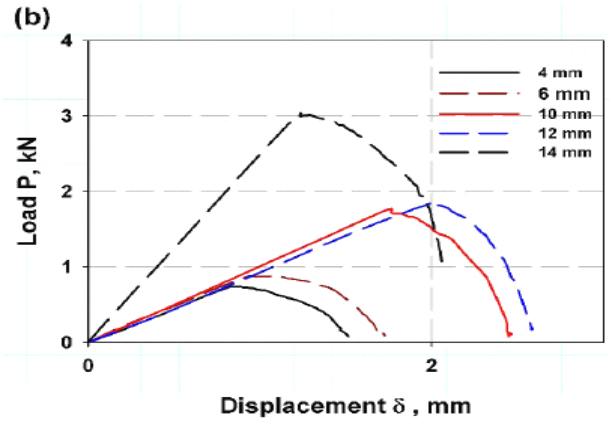


**Fig.6 Load Displacement curve for DENTof ;**
**(a) 5mm thickness, (b) 1.8 mm thickness**

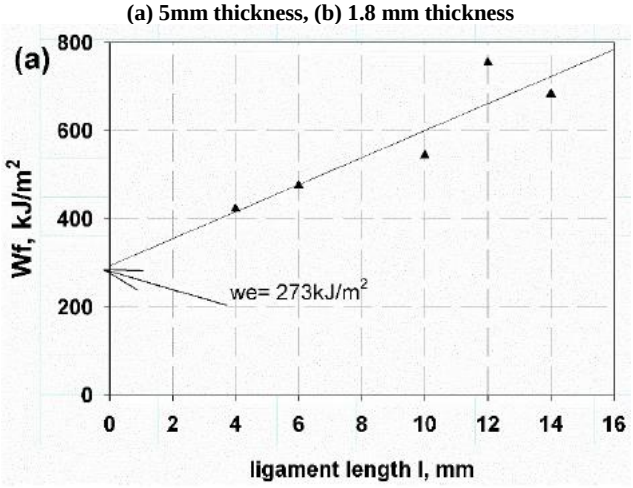


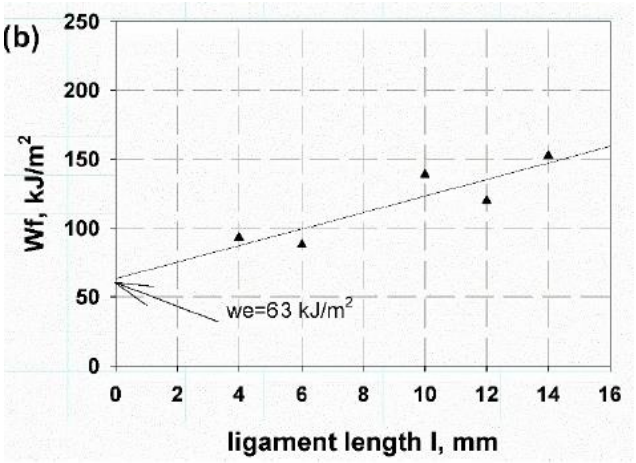


**Fig .7 EWF fitting for DENT of;**
**(a)5 mm thickness, (b) 1.8 mm thickness**

### 6.2. Strain rate

The EWF of 5 mm specimens measured at room temperature from strain rate experimental test at a deformation speed of 5 mm/min the curves of ligaments 4, 6, 10, 12, and 14 demonstrate linear growth up .The greatest load is shown around ligament yielding, and after reaching the peak point (full yield), these carvings continue to rise linearly until necking is seen. Then there is ductile tearing, and finally there is a sudden failure.

Figure 8.(a) and (b) depicts a peak point at the maximum load followed by necking. The next step is ductile ripping, and the last is failure. Similar geometries can be seen in the load-displacement curves as a function of ligament length. The area under the load-displacement curve is a measure of the overall energy stored in the broken specimen. Eq(1) is used to calculate this area . The increase in the amount of material to be deformed is what causes the internal work to grow as the ligament length does. After that, the crack advances through the material against an increasing resistance (increasing fracture process zone length is observed with increasing ligament length). A decrease in the pre-crack length (a) is implied by an increase in ligament length.

We can see in Figs. 9. (a) And (b) a linear fitting was used to analyses the relationship between wf and ligament lengths. The results obtained show that EWF can be used with the test material. 330 kJ/m2 for 5 mm and 28 kJ/m2 for 1.8 mm are the values assigned to the EWF we. The point where the Y-axis intersects the ligament and the slope of the linear regression represents the non-essential work of fracture. Also the numbers show the impact of strain rate at EWF, where fracture requires excessive more energy for 5mm thickness and increasing cross-head speed increasing resistance of atomic bonds at ligament length creating a high localized stress at crack tip in addition to the volume of this specimen. So this result reinforces the stress raiser theory .But the thin thickness 1.8 mm appears more brittle and less energy requires to fracture due to the narrow crack surface having

little to no bridging by solid tiny particles of Mgo to the crack, the fracture toughness at the thin thickness was relatively low.

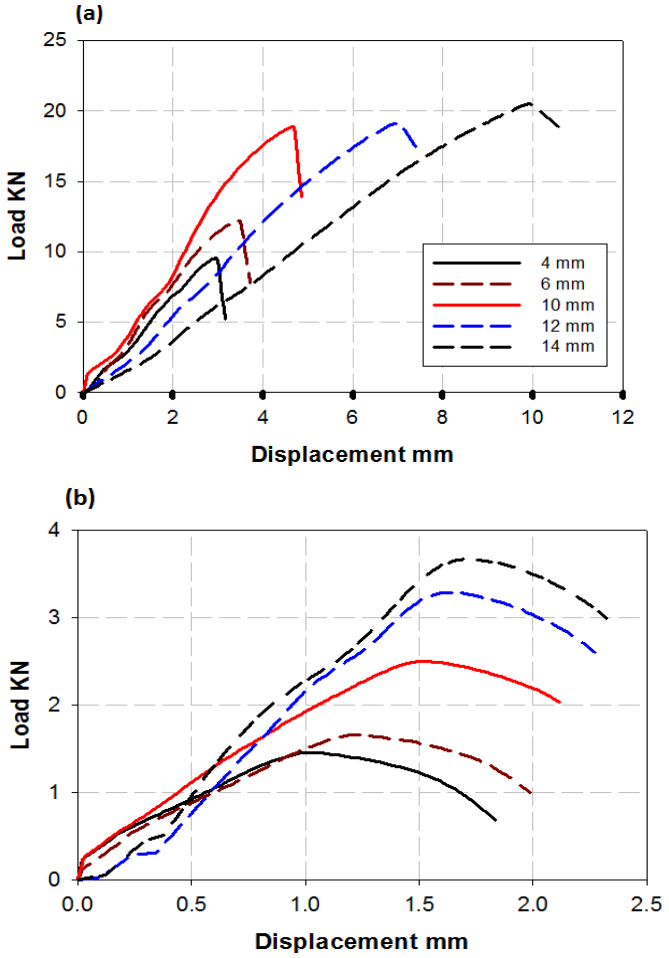


**Fig.8 Load Displacement curve for DENT of ; (a) 5mm thickness, (b) 1.8 mm thickness**

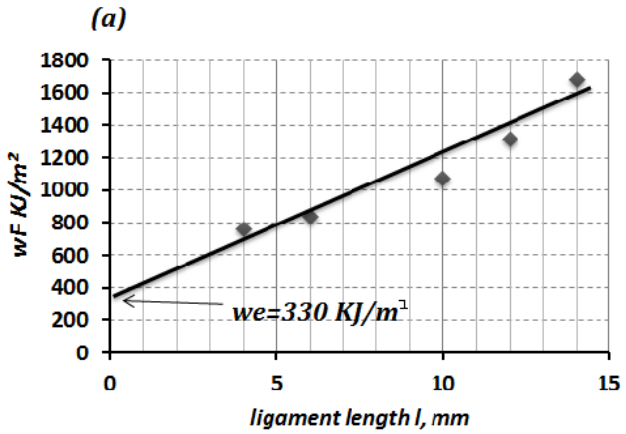


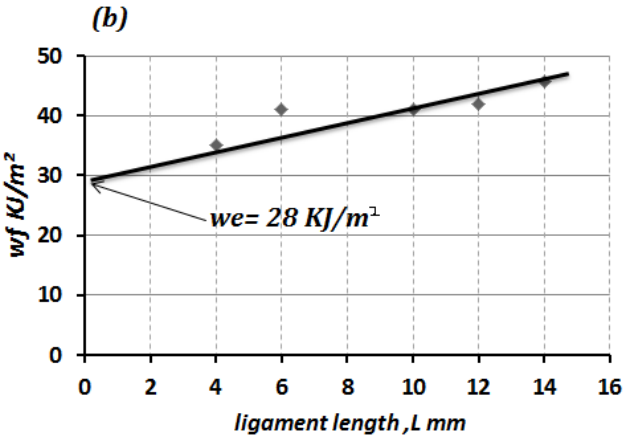


**Fig .9 EWF fitting for DENT of; (a)5 mm thickness, (b) 1.8 mm thickness**

### 6.2. Hole

The load-displacement curves obtained from the EWF of 5mm specimens measured at room temperature are shown in Fig. 8. a The ligaments 6, 10, 12, and 14 have curves that increase linearly up correspond to the yield region. The maximum load is seen around ligament yielding, and then necking is seen. These carvings keep getting bigger until they reach their peak point (full yield). Then comes ductile ripping, and then curvature failure comes last.

The maximum load is shown in Fig. 8. (b) as a peak point, followed by necking. Failure comes next, which is followed by ductile ripping. The geometry of the load-displacement curves as a function of ligament length is comparable. The area under the load-displacement curve represents the overall energy that was stored in the broken specimen. Using Eq(1), this area is quantified . Due to the increased amount of material that needs to be bent, the internal work rises as ligament length does. Increasing resistance causes the crack to continue to spread through the material (increasing fracture process zone length is observed with increasing ligament length). Increases in ligament length imply decreases in pre-crack length (a), and vice versa.

The relationship between $W_f$ and ligament lengths was fitted linearly, as can be seen in Fig. 9. (a) and(b). The obtained results show that EWF can be used with the test material. 380 kJ/m2 for 5mm and 110 kJ/m2 for 1.8 mm are the EWF values that are measured. As shown in Figs. 9. (a) And (b), it is the intercept with the Y-axis at zero ligament length, and the slope of the linear regression represents the non-essential work of fracture. It is noteworthy that during the stress wave propagation in the material, the crack's propagating velocity was significantly lowered as it neared the holes; the particles were stimulated by the stress wave with various velocities. The particles on the free surface were unrestrained and migrated forward when the stress wave hit the surfaces of the holes, deforming the holes. The amplitude and

direction of the particle velocities between the holes and the crack tip altered together with the crack tip's extension. As a result, the crack propagation behavior was affected and the state mobility of the particles in the crack tip changed. The effect of the holes was dependent on the compressive stress field caused by the particle movement during the crack propagation process. It can be seen that the particles in the running crack tip were restrained when the crack rushed into the holes' zone, lasting until the crack escaped the zone. These figures thus demonstrate a decrease in the influence of the hole at the EWF,which requires more energy to fracture, and an increase in the stress concentration at the crack tip.

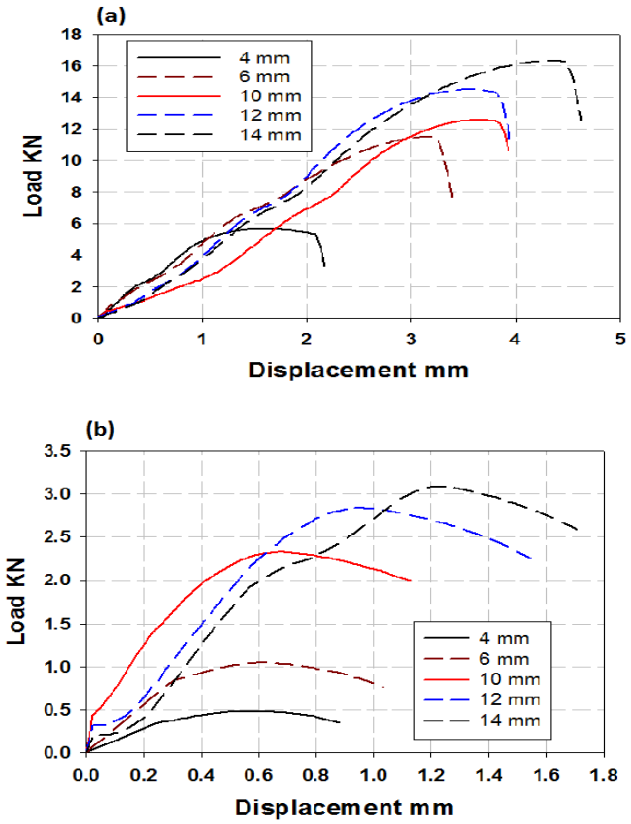


**Fig.10. Load Displacement curve for DENT of ; (a) 5mm thickness, (b) 1.8 mm thickness**

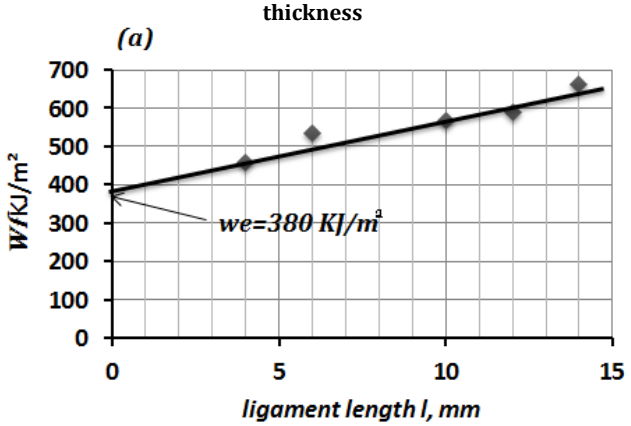


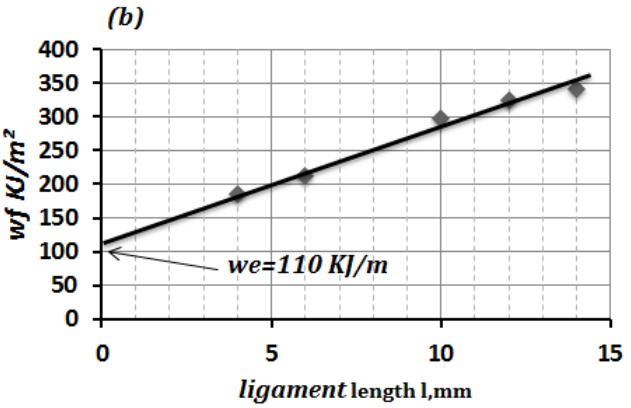


**Fig.11. EWF fitting for DENT of; (a)5 mm thickness, (b) 1.8 mm thickness**

### 6.2. Pre-stress

These values were calculated as 20% from the ultimate stress measurement at room temperature by applying 4.97 KN at 5 mm specimens and 0.64 KN at 1.8 mm specimens. Fig.10. (a) Depicts the behavior of 5 mm specimens of ligaments 6, 10, 12, and 14 as they increase linearly until the full yield region. The highest load is seen around ligament yielding, and after reaching the peak point (full yield), these carvings start to neck. The next step is ductile ripping, and the last is curvature failure.

Fig.10. (b) depicts the behavior of 1.8 mm specimens of ligaments 12, 14, which exhibit linear growth up to a point at which oscillations starts to develop and are said to be related to the yield area. The maximum load is seen around ligament yielding, and then necking is seen. These carvings keep getting bigger until they reach their peak point (full yield). Then there occurs ductile ripping, and the process ends with a significant curvature failure.

The relationship between $W_f$ and ligament lengths was fitted linearly, as can be seen in Fig. 11. (a) and(b). The obtained results show that EWF can be used with the test material. 250 kJ/m2 for 5mm and 20 kJ/m2 for 1.8 mm are the EWF values that are measured. As shown in Figs. 11.(a) and (b), it is the intercept with the Y-axis at zero ligament length, and the slope of the linear regression represents the non-essential work of fracture.

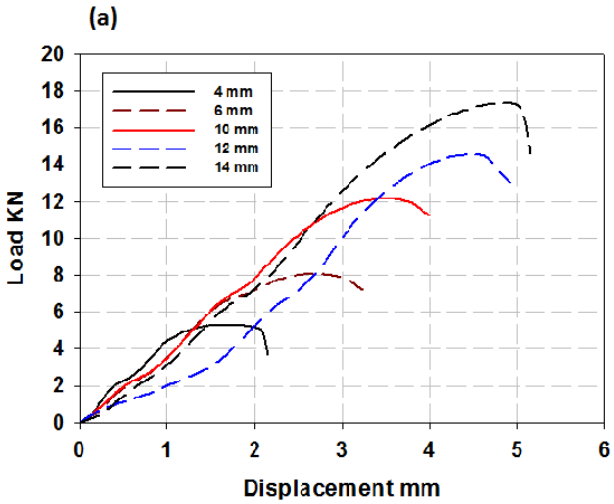


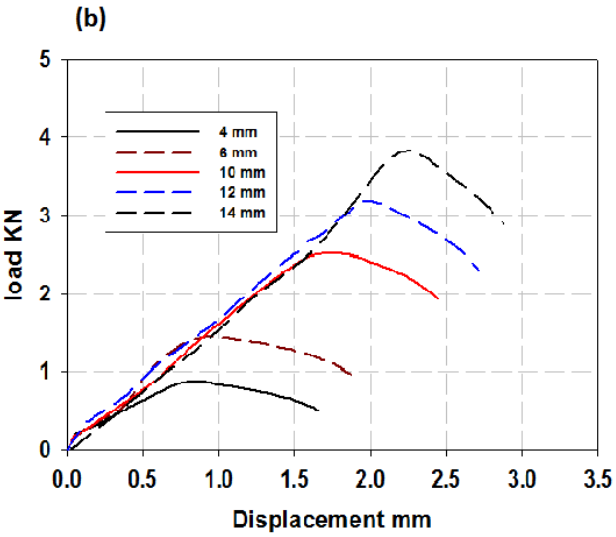


**Fig.12. Load Displacement curve for DENT of ;**
**(a) 5mm thickness, (b) 1.8 mm thickness**

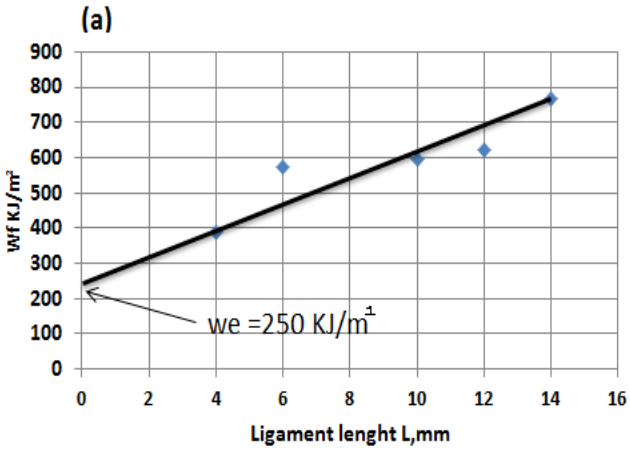


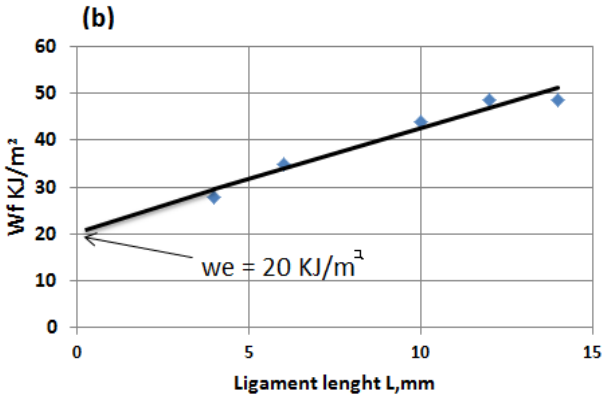


**Fig.13. EWF fitting for DENT of;**
**(a)5 mm thickness, (b) 1.8 mm thickness**

These values were calculated as 30% from the ultimate stress measurement at room temperature by applying 7.45 KN at 5 mm specimens and 0.97 KN at 1.8 mm specimens. A linear increase in behavior is shown in Fig. 11. (a )for 5 mm specimens of ligaments 6, 10, 12, and 14 up. The maximum load is seen around ligament yielding, and then necking is seen. These carvings keep getting bigger until they reach their peak point (full yield). After that, ductile ripping occurs, and then curvature failure follows.
Fig.11.(b) depicts the behavior of 1.8 mm specimens of ligaments 10, 12, and 14 as they increase linearly. The maximum load is seen around ligament yielding, and then necking is seen. These carvings keep getting bigger until they reach their peak point (full yield). The next step is ductile ripping, and the last is a medium curvature failure.

The relationship between $W_f$ and ligament lengths was fitted linearly, as can be seen in Fig. 9. (a) and(b). The obtained results show that EWF can be used with the test material. 230 kJ/m2 for 5 mm and 15 kJ/m2 for 1.8 mm are the EWF values that are measured. As shown in Figs. 9. (a) And (b), it is the intercept with the Y-axis at zero ligament length, and the slope of the linear regression represents the non-essential work of fracture. These numbers show that the influence of the increasing the pre-load applied at the EWF, which requires less energy for fracture.

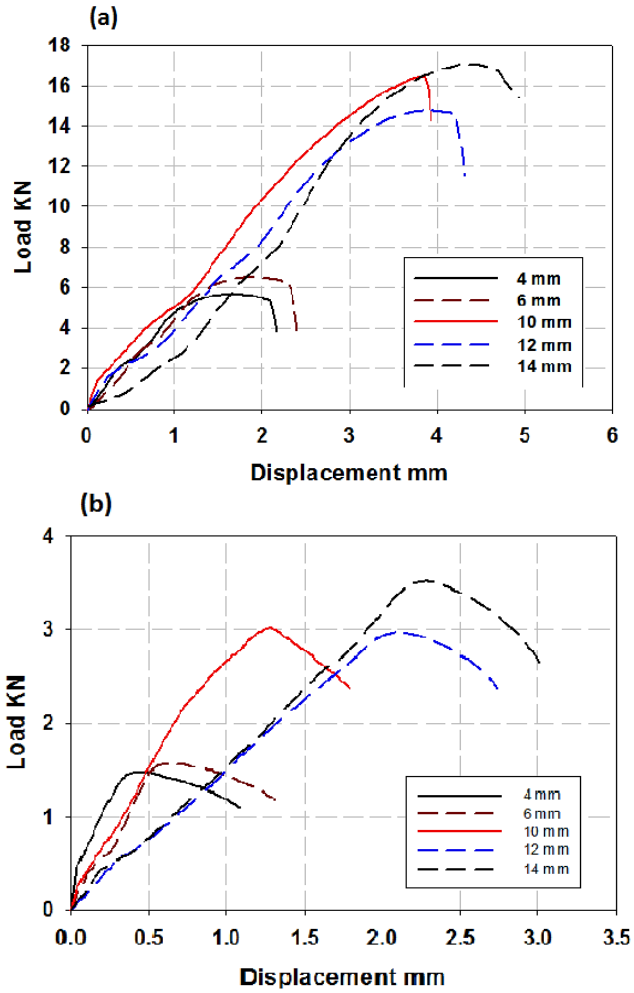


**Fig.14 Load Displacement curve for DENT of ;**
**(a) 5mm thickness, (b) 1.8 mm thickness**

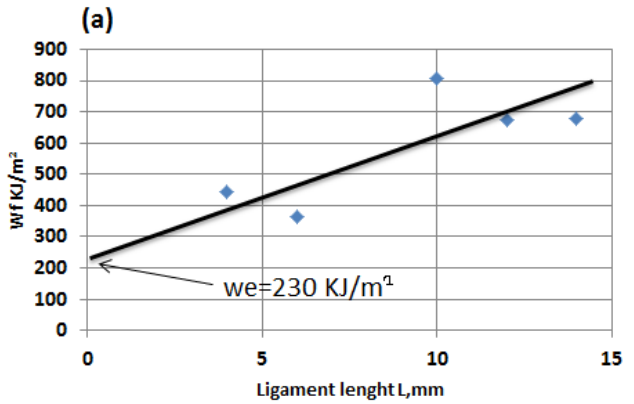


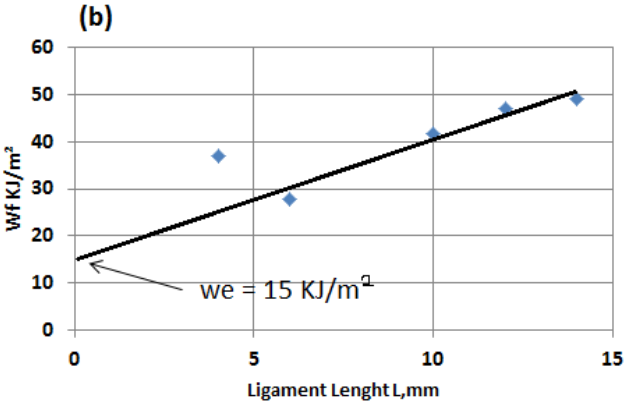


**Fig.15 EWF fitting for DENT of;**
**(a)5 mm thickness, (b) 1.8 mm thickness**

Applying 9.94 KN to 5 mm specimens and 1.29 KN to 1.8 mm specimens resulted in estimates of these values that represent 40% of the ultimate stress measured at room temperature. The behavior of 5mm specimens of the ligaments 6, 10, 12, and 14 is depicted in Fig. 12. (a) As linear growth up. The maximum load is seen around ligament yielding, and then necking is seen. These carvings keep getting bigger until they reach their peak point (full yield). Then comes ductile ripping, and then curvature failure comes last.

Figure.12. (b) depicts the behavior of ligament specimens measuring 1.8 mm, showing a linear increase up. The highest load is seen around ligament yielding, and after reaching the peak point (full yield), these carvings start to neck. Ductile ripping comes next, and the failure has a medium curvature after that.

The relationship between $W_f$ and ligament lengths was fitted linearly, as can be seen in Fig. 9. (a) and(b). The obtained results show that EWF can be used with the test material. 210 kJ/m2 for 5mm and 10 kJ/m2 for 1.8 mm are the EWF values that are measured. As shown in Figs. 9.(a) and (b), it is the intercept with the Y-axis at zero ligament length, and the slope of the linear regression represents the non-essential work of fracture. These numbers show that the influence of the increasing the pre-load applied at the EWF, which requires less energy for fracture.

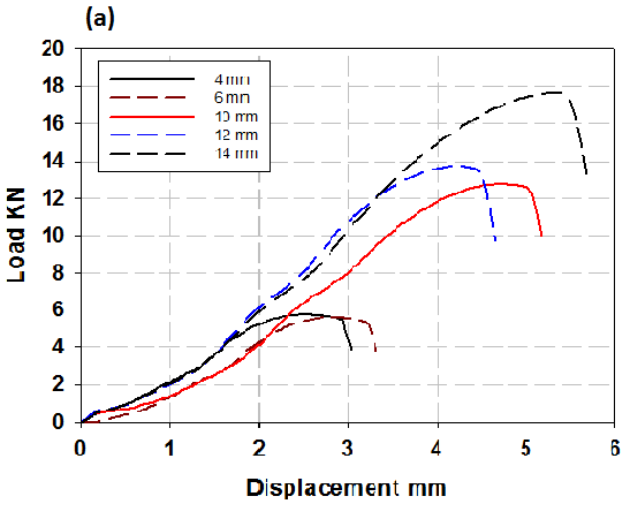


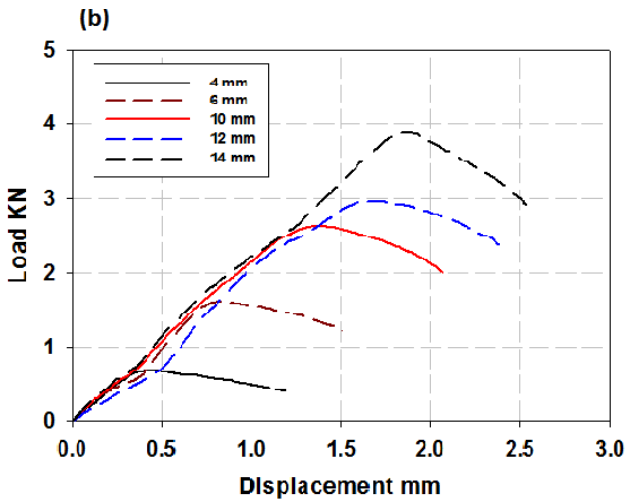


**Fig.16 Load Displacement curve for DENT of ;**
**(a) 5mm thickness,(b) 1.8 mm thickness**

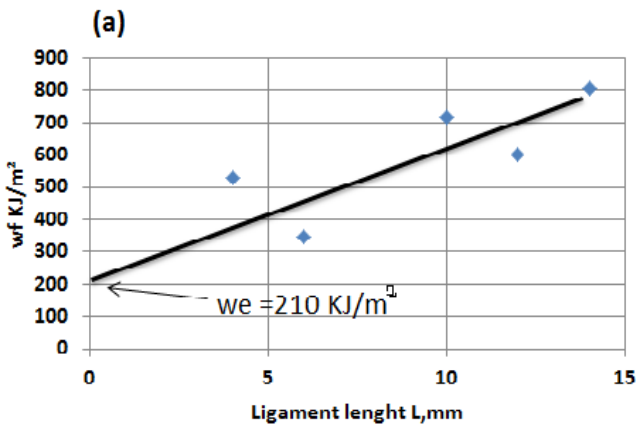


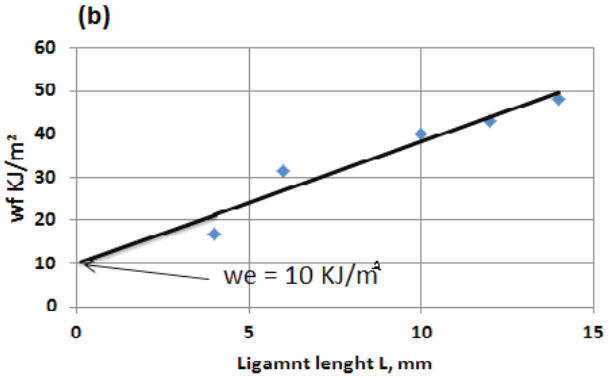


**Fig.17. EWF fitting for DENT of;**
**(a)5 mm thickness, (b) 1.8 mm thickness**

By applying 12.4 KN to 5 mm and 1.6 KN to 1.8 mm specimens, these values were estimated to be 50% of the ultimate stress measured at ambient temperature. Figure 29 depicts the behavior of 5 mm specimens of the ligaments 6, 10, 12, and 14 as they increase linearly up until a particular point at which oscillations start to develop and are said to be related to the yield region. The highest load is shown around ligament yielding as these carvings continue to grow until they reach their peak point (full yield), after which necking is seen. Curvature failure comes next, then ductile ripping. The relationship between $W_f$ and ligament lengths was fitted linearly, as can be seen in Fig. 9. (a) and(b). The obtained results show that EWF can be used with the test material. 190 kJ/m2 for 5mm the EWF value that measured as shown in Figs. 9.(a) and (b), it is the intercept with the Y-axis at zero ligament length, and the slope of the linear regression represents the non-essential work of fracture. These numbers show that the influence of the increasing the pre-load applied at the EWF, which requires less energy for fracture.

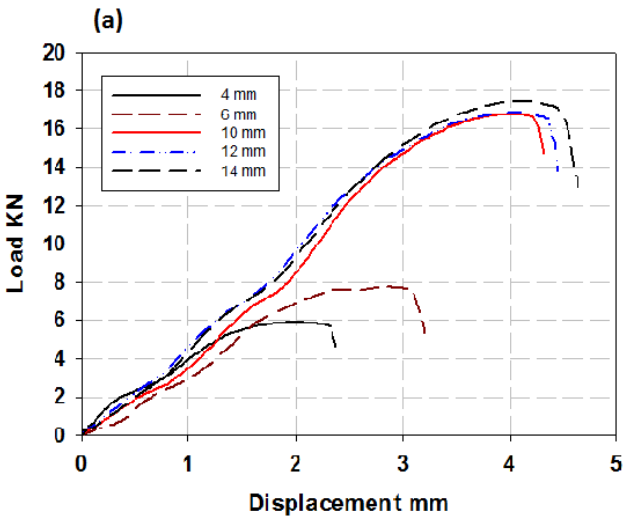

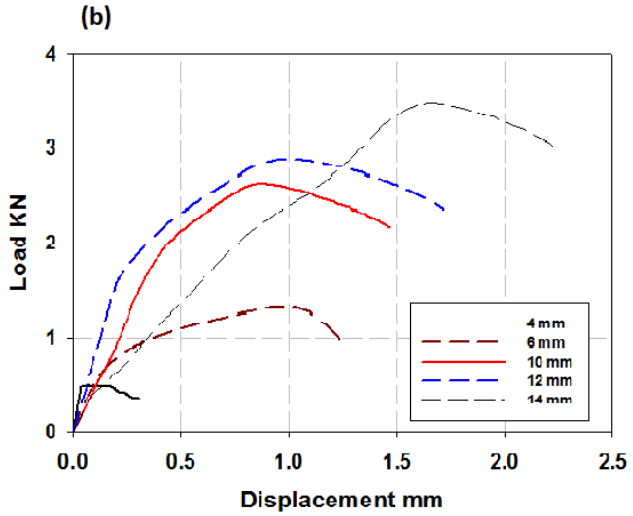


**Fig.18 Load Displacement curve for DENT of; (a) 5mm thickness, (b) 1.8 mm thickness**

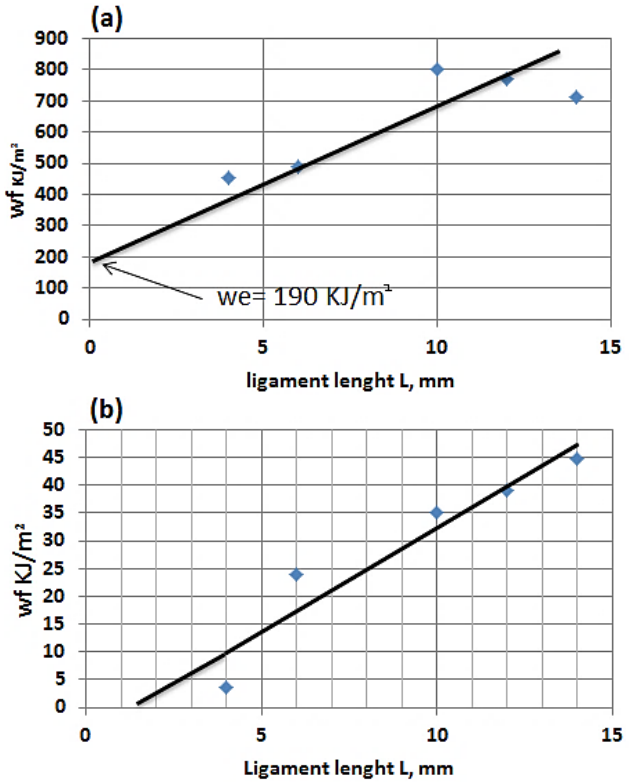


**Fig.19 EWF fitting for DENT of; (a)5 mm thickness, (b) 1.8 mm thickness**


**(a) 5mm thin-plate aluminum specimen**

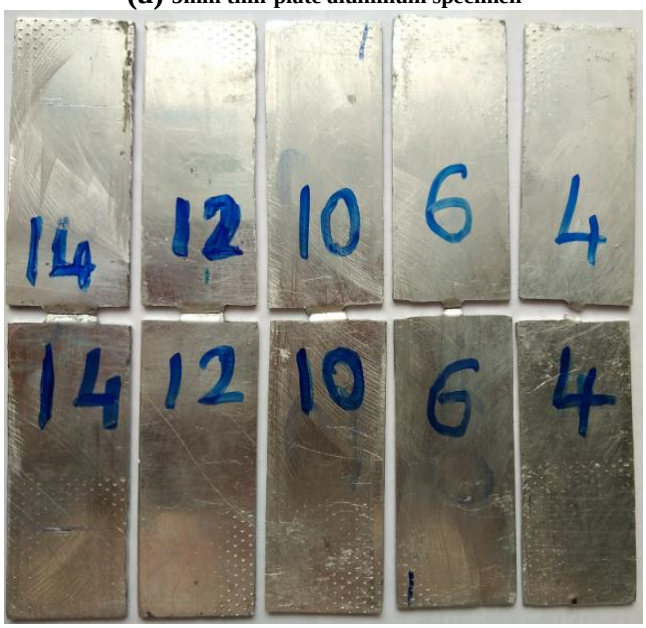


**(b) 1.8mm thin-plate aluminum specimen**

**Fig. 20. Modes of failure of EWF**


**(a) 5mm thin-plate aluminum specimen**

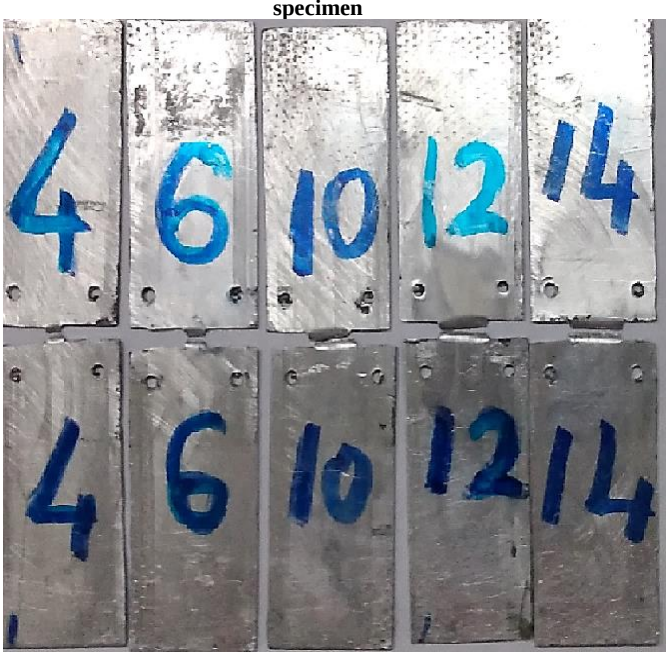


**(b)1.8mm thin-plate aluminum specimen**

**Fig. 21 Modes of failure of hole**

## 7. Comparison of the study cases.

The Essential Work of Fracture (EWF) approach is one of the few experimental methods to evaluate the fracture toughness of highly ductile materials under plane-stress conditions (thin films or sheets) based on the stored energy of the body. Feasibility of Stress raiser has been created as a result of critical defects as holes, changes in stiffness, sharp corners and cracks. Most of stress riser fractures occur in regions where stress forces are higher than those in the surrounding material. Most stress riser fractures are related to technical errors (iatrogenic causes) and are difficult to manage ,So the crucial work effect of stress raiser appear in strain rate and hole procedures which propagations shield other potential fracture origins from initiation induce a localized stress at crack tip improved a higher measurement values appeared at essential work of fracture .Furthermore the procedure of pre-stress contribute to make more dimples and void coalescence that effect on the cohesive energy of particles .This great effect on material behavior attributes on the atomic bonds broken and contributes to be reducing the material toughness.

The results achieved a gradually values for two thickness, holes procedures and strain rate the top due to localized stress at crack tip as mentioned before. On the other hand, the pre-load weakened the molecules bonds. We can present the results in the following table [3]:

| Procedures | EWF for 5mm ($KJ/m^2$) | EWF for 1.8mm ($KJ/m^2$) |
|---|---|---|
| Hole | 380 | 110 |
| Strain Rate | 330 | 28 |
| EWF | 273 | 63 |
| Pre-stress 20% | 250 | 20 |
| Pre-stress 30% | 230 | 15 |
| Pre-stress 40% | 210 | 10 |
| Pre-stress 50% | 190 | |

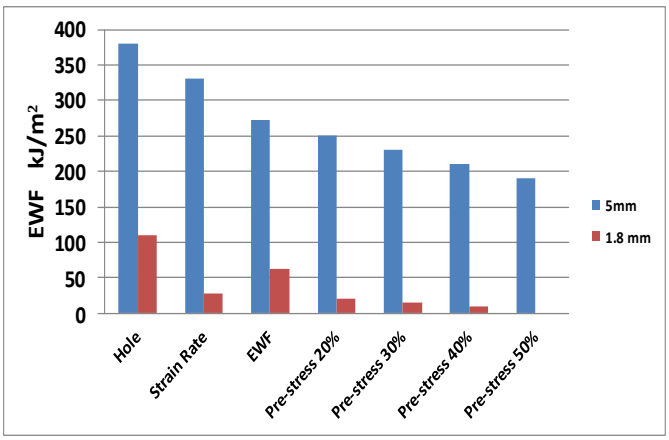


**Fig 22. Comparably chart of stress raiser procedure**

## 8. Conclusion:

This study focus on the behavior of engineering materials containing abrupt cracks, notches, or points of immediately concentrated load. The investigation of this study is to develop the theory of the fracture to A5754 aluminum alloy, consistent with the existing theories and experimental observations of their behavior by using three phase of

fracture dealing with stress concentration applications which affected on the grain boundaries and crystals orientation. The EWF method achieved 273 KJ/m² for 5 mm thickness and 63 KJ/m² for 1.8 mm. On the other side strain rate which give 330 kJ/m²for 5mm and 28 kJ/m²for1.8 mm. By applying holes near the crack the toughness increased which has been presented at the high value of EWF measurement compared without holes that the 5 mm specimen's thickness achieves 380 KJ/m² and for 1.8 mm thickness 110 KJ/m. The procedure of pre-stress 20% give EWF measured values 250 kJ/m²for 5mm and 25 kJ/m²for1.8 mm, pre-stress 30% EWF measured 230 kJ/m²for 5mm and 15 kJ/m²for1.8 mm, pre-stress 40%The EWF measured 210 kJ/m²for 5mm and 10 kJ/m²for1.8 mm. And pre-stress 50% the EWF achieve lowest value measured as 190 kJ/m²for 5mm and. These tests have a great practical effect on ductility due to cohesive energy release. This energy improved at provides holes near crack tips which reduce stress concentration and the impact high speed operated on tension test. On other hand by applying pre-load procedure the atomic bonds have been broken to reach the plastic zone.

## References:


1. Burger, G., et al., Microstructural control of aluminum sheet used in automotive applications. Materials Characterization, 1995. **35**(1): p. 23-39.
2. Gertsman, V., et al., EBSD study of microstructure evolution in model aluminum alloys during annealing and high-temperature deformation. 2001.
3. Broberg, K., Critical review of some theories in fracture mechanics. International Journal of Fracture Mechanics, 1968. **4**: p. 11-19.
4. Broberg, K., Crack-growth criteria and non-linear fracture mechanics. Journal of the Mechanics and Physics of Solids, 1971. **19**(6): p. 407-418.
5. Broberg, K., On stable crack growth. Journal of the Mechanics and Physics of Solids, 1975. **23**(3): p. 215-237.
6. Abdellah, M.Y., et al., Ductile fracture toughness of Al 5754-H111 alloy using essential work of fracture method. AIMS Materials Science, 2023. **10**(2): p. 370-389.
7. Abdellah, M.Y., Essential work of fracture assessment for thin aluminium strips using finite element analysis. Engineering Fracture Mechanics, 2017. **179**: p. 190-202.
8. Betegon, C., C. Rodriguez, and F. Belzunce, Analysis and modelisation of short crack growth by ductile fracture micromechanisms. Fatigue & Fracture of Engineering Materials & Structures, 1997. **20**(5): p. 633-644.
9. Cadoni, E., et al., Effects of strain rate on mechanical properties in tension of a commercial aluminium alloy used in armour applications. Procedia Structural Integrity, 2016. **2**: p. 986-993.
10. Rizal, S., et al., Influences of strain rate on yield strength aluminum alloys. Proceedings of SPIE - The International Society for Optical Engineering, 2005. **5852**.
11. Singh, N., et al., Strain Rate Sensitivity of an Aluminium Alloy under Compressive Loads. Advanced Materials Research, 2012. **548**.
12. Singh, N., et al., Dynamic Characteristics of Aluminium Alloys at Wide Range of Strain Rates. Proceedings of the Indian National Science Academy, 2013. **79**: p. 587.
13. Tanimura, S., et al., Dynamic tensile properties of steels and aluminum alloys for a wide range of strain rates and strain. Journal of Solid Mechanics and Materials Engineering, 2009. **3**(12): p. 1263-1273.
14. Oosterkamp, L.D., A. Ivankovic, and G. Venizelos, High strain rate properties of selected aluminium alloys. Materials Science and Engineering: A, 2000. **278**(1-2): p. 225-235.
15. Chen, Y., et al., Stress–strain behaviour of aluminium alloys at a wide range of strain rates. International Journal of Solids and Structures, 2009. **46**(21): p. 3825-3835.
16. Hirano, K. Ultra-high temperature testing methodologies for functionally gradient materials. in Proc. of 1st Int. Symp. on FGMs. 1990.
17. Sburlati, R., S.R. Atashipour, and S.A. Atashipour, Reduction of the stress concentration factor in a homogeneous panel with hole by using a functionally graded layer. Composites Part B: Engineering, 2014. **61**: p. 99-109.
18. Saini, P.K. and M. Kushwaha, Stress variation around a circular hole in functionally graded plate under bending. International Journal of Mechanical and Mechatronics Engineering, 2014. **8**(3): p. 538-542.
19. Song, P. and Y. Shieh, Stop drilling procedure for fatigue life improvement. International Journal of Fatigue, 2004. **26**(12): p. 1333-1339.
20. Ghfiri, R., et al., Fatigue life estimation after crack repair in 6005 A-T6 aluminium alloy using the cold expansion hole technique. Fatigue & Fracture of Engineering Materials & Structures, 2000. **23**(11): p. 911-916.
21. Abdellah, M.Y., et al., Finite Element Analysis of Vibration modes in Notched Aluminum Plate. Journal of Mechanical Engineering Research and Developments, 2021. **44**(10): p. 343-353.
22. Zhu, Z., B. Mohanty, and H. Xie, Numerical investigation of blasting-induced crack initiation and propagation in rocks. International Journal of Rock Mechanics and Mining Sciences, 2007. **44**(3): p. 412-424.
23. Zhu, Z., Numerical prediction of crater blasting and bench blasting. International Journal of Rock Mechanics and Mining Sciences, 2009. **46**(6): p. 1088-1096.
24. Wang, M., et al., Study of mixed-mode I/II fractures using single cleavage semicircle compression specimens under impacting loads. Engineering Fracture Mechanics, 2017. **177**: p. 33-44.
25. Wang, M., et al., Modelling of crack propagation in rocks under SHPB impacts using a damage method. Fatigue & Fracture of Engineering Materials & Structures, 2019. **42**(8): p. 1699-1710.
26. Zhu, Z., et al., Study on the mechanism of zonal disintegration around an excavation. International Journal of Rock Mechanics and Mining Sciences, 2014. **67**: p. 88-95.
27. Wang, F. and M. Wang, Effect of holes on dynamic crack propagation under impact loading. Applied Sciences, 2020. **10**(3): p. 1122.
28. Abi-Akl, R. and D. Mohr, Paint-bake effect on the plasticity and fracture of pre-strained aluminum 6451 sheets. International Journal of Mechanical Sciences, 2017. **124**: p. 68-82.
29. Furu, T., O. Ryen, and O. Myhr. Effect of pre-deformation on age hardening kinetics i n commercial 6xxx alloys. in Proc. 11th Intern. Conf. Aluminium Alloys. 2008.
30. Granum, H., et al., Effect of pre-stretching on the mechanical behaviour of three artificially aged 6xxx series aluminium alloys. Materials Today Communications, 2021. **27**: p. 102408.

31. Al-Rubaie, K.S., et al., Effect of pre-strain on the fatigue life of 7050-T7451 aluminium alloy. Materials Science and Engineering: A, 2007. **464**(1-2): p. 141-150.
32. Branco, R., et al., Effect of tensile pre-strain on low-cycle fatigue behaviour of 7050-T6 aluminium alloy. Engineering Failure Analysis, 2020. **114**: p. 104592.
33. Froustey, C. and J.L. Lataillade, Influence of large pre-straining of aluminium alloys on their residual fatigue resistance. International journal of fatigue, 2008. **30**(5): p. 908-916.
34. Abdellah, M.Y., Ductile Fracture and S–N Curve Simulation of a 7075-T6 Aluminum Alloy under Static and Constant Low-Cycle Fatigue. journal of failure analysis and prevention, 2021. **21**(4): p. 1476-1488.
35. White, B., et al., The effect of tensile pre-straining on fatigue crack initiation mechanisms and mechanical behavior of AA7050 friction stir welds. Materials Science and Engineering: A, 2018. **736**: p. 228-238.
36. Chiou, Y.-C. and J.-K. Yang, The effects of pre-deformation on the subsequent fatigue behaviors of SUS 430 Stainless Steel in load-control. International Journal of Solids and Structures, 2012. **49**(23-24): p. 3263-3268.
37. Sun, H., et al., Effects of pre-strain and annealing on the fatigue properties of complex phase steel CP800. International Journal of Fatigue, 2020. **131**: p. 105364.
38. Demiray, Y., Z. Kavaklioglu, and O. Yucel, A Study on Thermo-Mechanical Behavior of AA5754 Alloy (Tread and Plain Sheet) Produced by Twin-Roll Casting. Acta Physica Polonica A, 2015. **127**(4): p. 1097-1099.
39. Rodríguez-Millán, M., et al., Experimental study on the perforation process of 5754-H111 and 6082-T6 aluminium plates subjected to normal impact by conical, hemispherical and blunt projectiles. Experimental Mechanics, 2014. **54**: p. 729-742.
40. ASTM, E., 399. Standard Test Method for Plane-Strain Fracture Toughness of Metallic Materials, Annual Book of ASTM Standards, 1997. **3**: p. 01.
41. Shinde, P.S., et al., Fracture toughness of thin aluminum sheets using modified single edge notch specimen. IJEIT, 2012. **1**: p. 283-288.
42. Kuno, T., et al., Deformation mechanism under essential work of fracture process in polycyclo-olefin materials. Express Polym Lett, 2008. **2**: p. 404-412.
43. Abdellah MY, Z.A., Azam SA, et al. , A comparative study to evaluate the essential work of fracture to measure the fracture toughness of quasi-brittle material. Materials Characterization, 2022. **15**: p. 4514.
44. Hassan MK, A.M., ElAbiadi TS, et al, Essential work of fracture and size effect in copper/glass-reinforced epoxy laminate composites used as MEMS devices. Am J Mech Eng, 2017. **5**: p. 234-238.
45. Cotterell, B. and J. Reddel, The essential work of plane stress ductile fracture. International journal of fracture, 1977. **13**: p. 267-277.
46. Noda, N.-A., et al., Strain rate concentration factor for flat notched specimen to predict impact strength for polymeric materials. Mechanics of Materials, 2019. **131**: p. 141-157.
47. Santos, A. Determination of stress concentration factors on flat plates of structural steel. in Journal of Physics: Conference Series. 2013. IOP Publishing.
48. Yilmaz, S., T. Yilmaz, and B. Kahraman, Essential work of fracture analysis of short glass fiber and/or calcite reinforced ABS/PA6 composites. Polymer Engineering & Science, 2014. **54**(3): p. 540-550.
49. Mai, Y.-W. and B. Cotterell, On the essential work of ductile fracture in polymers. International journal of fracture, 1986. **32**: p. 105-125.
50. Yilmaz, S., T. Yilmaz, and A. Armagan Arici, Effect of annealing process in water on the essential work of fracture response of ultra high molecular weight polyethylene. Journal of materials science, 2011. **46**: p. 1758-1766.
51. Hashemi, S., Work of fracture of high impact polystyrene (HIPS) film under plane stress conditions. Journal of materials science, 2003. **38**: p. 3055-3062.
52. Warren, J., T. Lacy, and J. Newman Jr, Validation of the Two-Parameter Fracture Criterion using 3D finite-element analyses with the critical CTOA fracture criterion. Engineering Fracture Mechanics, 2016. **151**: p. 130-137.
53. Dhingra, A.K. and S.G. Fishman, Interfaces in metal-matrix composites; Proceedings of the Symposium, New Orleans, LA, Mar. 4-6, 1986, in Conference: 115. American Institute of Mining, Metallurgical and Petroleum Engineers annual meeting, New Orleans, LA, USA, 2 Mar 1986. 1986, Metallurgical Society, Inc.,Warrendale, PA: United States. p. Medium: X; Size: Pages: 263.
54. Abdellah, M.Y., et al., Experimental Evaluation of Mechanical and Tribological Properties of Segregated Al-Mg-Si Alloy Filled with Alumina and Silicon Carbide through Different Types of Casting Molds. Metals, 2023. **13**(2): p. 316.